Nacre-Inspired Composite Electrolytes for Load-Bearing Solid-State Lithium-Metal Batteries

Aijun Li, Xiangbiao Liao, Hanrui Zhang, Lei Shi, Peiyu Wang, Qian Cheng, James Borovilas, Zeyuan Li, Wenlong Huang, Zhenxuan Fu, Martin Dontigny, Karim Zaghib, Kristin Myers, Xiuyun Chuan, Xi Chen,* and Yuan Yang*

Solid-state lithium-metal batteries with solid electrolytes are promising for next-generation energy-storage devices. However, it remains challenging to develop solid electrolytes that are both mechanically robust and strong against external mechanical load, due to the brittleness of ceramic electrolytes and the softness of polymer electrolytes. Herein, a nacre-inspired design of ceramic/polymer solid composite electrolytes with a "brick-and-mortar" microstructure is proposed. The nacre-like ceramic/polymer electrolyte (NCPE) simultaneously possesses a much higher fracture strain (1.1%) than pure ceramic electrolytes (0.13%) and a much larger ultimate flexural modulus (7.8 GPa) than pure polymer electrolytes (20 MPa). The electrochemical performance of NCPE is also much better than pure ceramic or polymer electrolytes, especially under mechanical load. A 5×5 cm^2 pouch cell with LAGP/poly(ether-acrylate) NCPE exhibits stable cycling with a capacity retention of 95.6% over 100 cycles at room temperature, even undergoes a large point load of 10 N. In contrast, cells based on pure ceramic and pure polymer electrolyte show poor cycle life. The NCPE provides a new design for solid composite electrolyte and opens up new possibilities for future solid-state lithium-metal batteries and structural energy storage.

The rapid-growing demands for portable electronics and electric vehicles have bolstered needs for next-generation lithium batteries with high energy density.[1–4] However, lithium batteries become more thermally vulnerable as energy density increases. Thermal runaway and explosion are prone to be triggered by failures such as mechanical damage and lithium dendrite growth inside batteries.[5,6] Nonflammable solid-state ceramic electrolytes (SSEs) provide alternatives to conventional flammable liquid electrolytes.[7–9] Various ceramic electrolytes with attractive ionic conductivities have been developed in the past two decades, including NASICON-type $Li_{1.5}Al_{0.5}Ge_{1.5}(PO_4)_3$ (LAGP),[10] $Li_{1.3}Al_{0.3}Ti_{1.7}(PO_4)_3$ (LATP),[11,12] garnet $Li_7La_3Zr_2O_{12}$ (LLZO),[13,14] and sulfides, such as $Li_{10}GeP_2S_{12}$ (LGPS)[15] and $Li_7P_3S_{11}$ (LPS).[16] These electrolytes also possess high modulus to help suppress lithium dendrite.[17,18] However, ceramic has low fracture resilience, making them vulnerable to external impact (e.g., nailing and shocking) and causing great challenges for scalable cell fabrication, particularly when its thickness is reduced to $\approx$10–20 µm to achieve high energy density. On the other side, polymer electrolytes (e.g., poly(ethylene oxide) (PEO)) are flexible and easy to process,[19] but they are not mechanically strong enough to suppress lithium dendrites, especially at high current density.[20,21] Their softness also makes them difficult to bear mechanical loads.

A. Li, H. Zhang, P. Wang, Dr. Q. Cheng, J. Borovilas, Z. Li, W. Huang,
Z. Fu, Prof. Y. Yang
Program of Materials Science and Engineering
Department of Applied Physics and Applied Mathematics
Columbia University
New York, NY 10027, USA
E-mail: yy2664@columbia.edu

A. Li, Prof. X. Chuan
Key Laboratory of Orogenic Belts and Crustal Evolution
School of Earth and Space Sciences
Peking University
Beijing 100871, China

Dr. X. Liao, Prof. X. Chen
Earth Engineering Center
Center for Advanced Materials for Energy and Environment
Department of Earth and Environmental Engineering
Columbia University
New York, NY 10027, USA
E-mail: xichen@columbia.edu

L. Shi, Prof. K. Myers
Department of Mechanical Engineering
Columbia University
New York, NY 10027, USA

M. Dontigny, Dr. K. Zaghib
IREQ-Institute Recherche d'Hydro-Québec
Varennes, Québec J3X 1S1, Canada

To address these challenges, polymer/ceramic composite electrolytes have been widely studied, where ceramic electrolytes are dispersed in a polymer matrix to enhance mechanical robustness. For example, nanoparticles,[22–24] nanofibers,[25–27] nanosheets,[28] aerogel,[29] and vertically aligned porous structure[30–32] of ceramic electrolytes have been explored. Although such composites increase the robustness of solid electrolytes, they come at the expense of significantly reduced mechanical modulus and strength compared to the pure ceramic electrolyte. For example, Young's modulus of only 0.43 GPa was reported in the silica-aerogel-reinforced composite electrolyte.[29] Moreover, as the polymer phase is typically more than 30% in volume[22,33] and solid polymer electrolyte has a much lower ionic conductivity ($<10^{-4}$ S cm^{-1} at room temperature (RT)), the addition of polymer electrolyte significantly reduces ionic conductivity of the composite.

To design solid electrolytes with simultaneously high mechanical modulus and excellent fracture resilience for withstanding the external impact of shocking and nailing,[34] we draw inspiration from the structure of natural nacre,[35] which is composed of a unique "brick-and-mortar" arrangement of brittle mineral $CaCO_3$ platelets and thin layers of protein polymer (**Figure 1**a). The staggered structure makes it one of the most efficient materials combining high strength and large toughness while remaining light overall.[36–39] Herein, inspired by the "brick-and-mortar" arrangement, we develop a versatile bottom-up approach to fabricate large-scale nacre-like solid electrolytes with ceramic electrolyte microplatelets as the "brick" and sticky polymer electrolytes as the "mortar", which aims to resolve the dilemma of mechanical robustness in pure ceramic or pure polymer electrolytes.

In this report, we demonstrate NCPEs with LAGP ceramic electrolyte combined with three types of polymer electrolytes, including PEO, poly(ether-acrylate) (PEA), and epoxy-based electrolytes. Compared to pure ceramic electrolytes, the NCPEs show slightly reduced ultimate flexural strength and higher fracture strain to accommodate external deformation. The LAGP–PEO NCPE possesses a high fracture strain of 1.1%, one order of magnitude larger than pure LAGP electrolyte (0.13%). Its flexural modulus also reaches 7.8 GPa. The assembled solid-state LiFePO$_4$ (LFP)/LAGP–PEO NCPEs/Li cell exhibits stable capacity retention of 92% for 300 cycles at 0.5 C. With the enhanced mechanical properties of NCPEs, the pouch cell of LFP/LAGP–PEA NCPEs/Li can provide steady power output, even under large external load of 10 N. On the other side, pouch cells with either pure polymer or pure ceramic electrolyte perform poorly under external load. This work provides a new design of solid-state electrolyte for solid-state lithium-metal batteries. Such a concept can also be used in structural energy storage,[40,41] where batteries with excellent mechanical properties replace structural components in vehicles and aircraft for weight reduction.

The bottom-up fabrication procedures of NCPEs are schematically shown in Figure 1b. A liquid suspension of ceramic electrolyte particles and polymer additives were coated onto a Mylar substrate (Step 1), and ceramic films after solvent evaporation were stacked and laminated together (Step 2). The freestanding films were then sintered at 850 °C to form a multilayered ceramic stack (Step 3), and subsequently soaked in polymer electrolyte dissolved in a solvent under vacuum. As a result, the polymer electrolyte is able to infiltrate the multilayer stack and stick to the ceramic surface (Step 4). The composite was then hot-pressed at 80 °C to break the ceramic electrolyte films into platelets and enable the polymer electrolyte to fill all gaps simultaneously, forming the nacre structure and further improving the contact between polymer and ceramic platelets
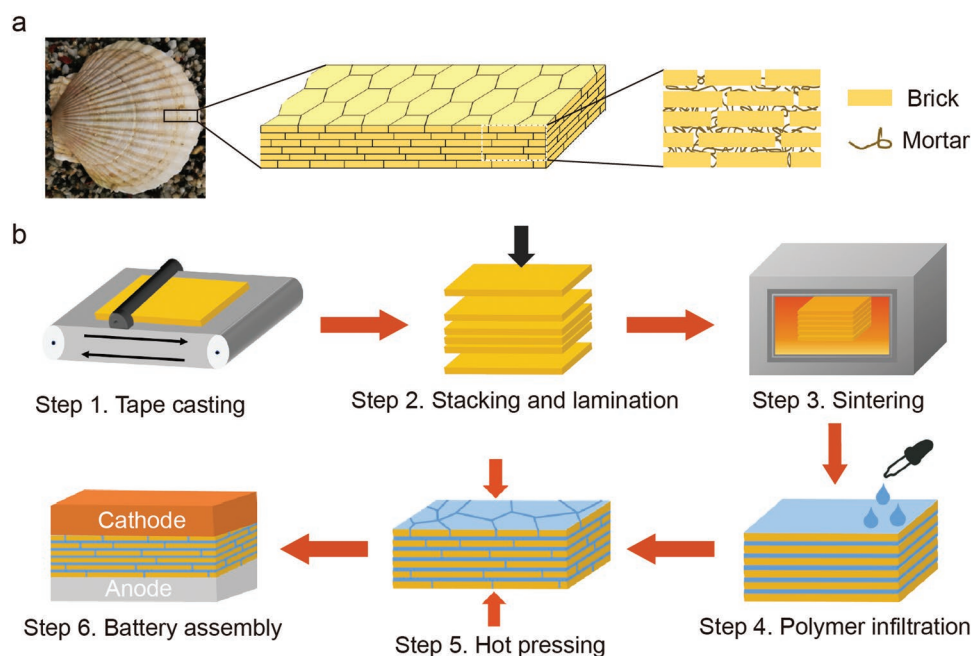
Figure 1. The design and fabrication of nacre-like ceramic/polymer composite electrolyte. a) Schematic of staggered "brick-and-mortar" microstructure in nacre. b) Schematic of the bottom-up fabrication process of NCPEs and battery assembly.
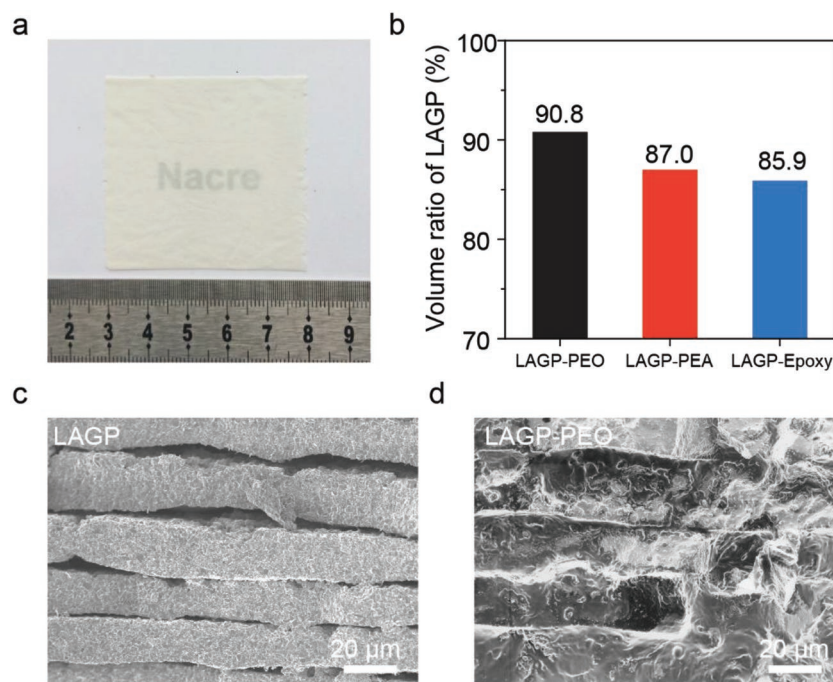
**ADVANCED
SCIENCE NEWS**

www.advancedsciencenews.com

**ADVANCED
MATERIALS**

www.advmat.de

(Step 5). The as-fabricated composite solid-state electrolyte was then assembled with a lithium-metal anode and LiFePO$_4$ cathode in a pouch cell configuration (Step 6). Such NCPE-based cell can serve as a promising dual-functional component for both energy storage units and load-bearing elements in various devices, such as vehicles and aircraft. This facile fabrication method can be extended to various ceramic/polymer materials, and herein, NCPEs of LAGP ceramic electrolyte with three different polymer electrolytes, PEO, PEA, and epoxy, are demonstrated. PEO is chosen as it is a low-cost, widely used polymer electrolyte.[30,42] PEA electrolyte is chosen to enable cycling at room temperature,[43] and epoxy electrolyte[44,45] is to further demonstrate versatility of the proposed process.

To demonstrate scalability, 5 cm × 5 cm NCPEs are prepared, with LAGP–PEO serving as an example (**Figure 2**a), wherein the translucent nature indicates large grain size and dense film since otherwise grain boundaries and pores will cause significant light scattering, rendering the film opaque. Thermal gravimetric analysis (TGA) indicates that the weight percentage of LAGP "brick" are 96.5%, 95.1%, and 94.4% for LAGP–PEO, LAGP–PEA, and LAGP–epoxy NCPEs, respectively (Figure S1, Supporting Information), corresponding to the volume portion of 90.8%, 87.0%, and 85.9%, respectively (Figure 2b). Besides large volume ratio of LAGP phase, the high crystallinity of LAGP and amorphous PEO (Figure S2 and Table S1, Supporting Information) also help retain high ionic conductivity in as-fabricated LAGP–PEO NCPEs. Scanning electron microscopy (SEM) images further confirm that ceramic microtablets are well aligned and closely packed, with the polymer electrolyte present between layers and inside gaps (Figure 2c,d). The

thickness and aspect ratio of as-fabricated individual LAGP tablets are ≈15 µm and 10–15, respectively, and the total thickness of the composite electrolyte is 100–200 µm. Such a large aspect ratio is critical to enhancing the mechanical strength and toughness of the nacre-like electrolyte.[38,39] The thickness of the cohesive PEO layer is ≈1 µm, which provides a soft but tough bridge between the brittle ceramic layers. A thin layer of PEO remains on the surface of the fabricated composite electrolyte (Figure S3, Supporting Information), which is critical for reducing interfacial resistance with lithium metal in assembled cells. Similar morphology and structure are also observed in LAGP–PEA and LAGP–epoxy NCPEs (Figure S4, Supporting Information). In the future, we expect that the thickness of individual tablet and entire electrolyte can be reduced to ≈3–5 and ≈10–20 µm after optimization, which is attractive for practical cells.
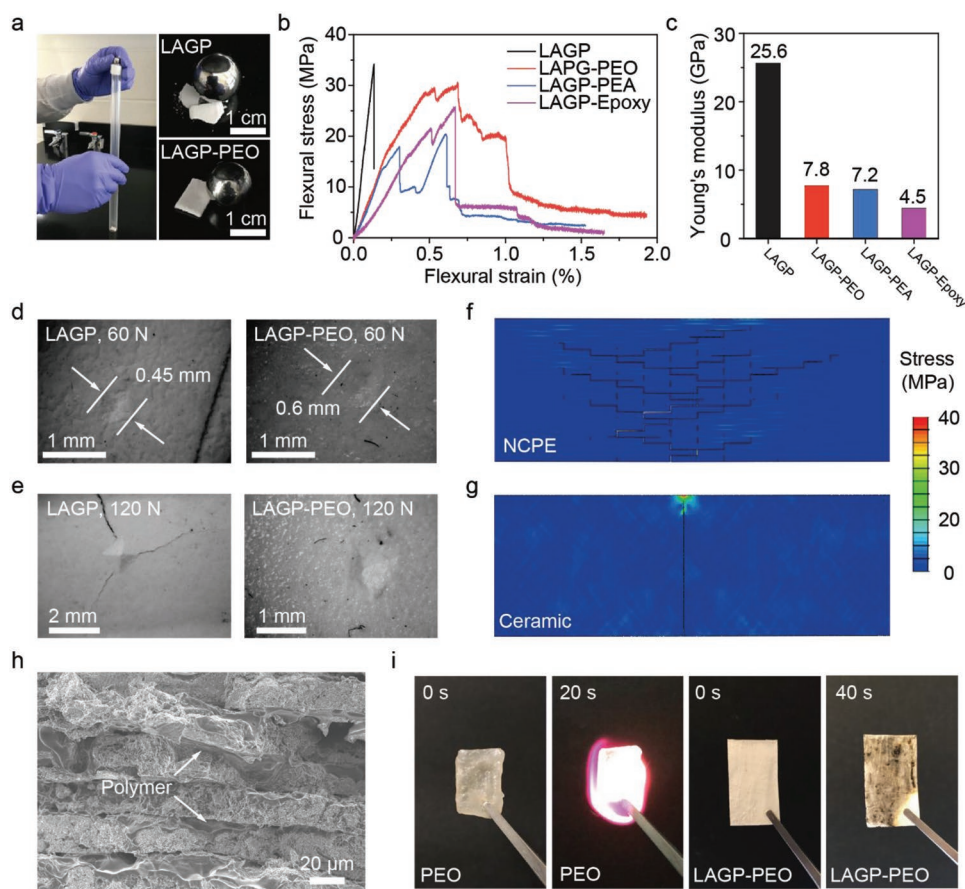
The as-fabricated NCPEs show significantly improved mechanical properties compared to pure ceramic and pure polymer electrolytes, as validated by ball impact, three-point bending, and indentation tests. All results show that NCPEs are much tougher than pure LAGP ceramic electrolyte, and have a much higher modulus than polymer electrolytes.

First, in ball impact tests, a stainless steel ball with a weight of 8.4 g is dropped from various heights onto the solid electrolyte. The pure LAGP film breaks into pieces when the ball is dropped from a height of 20 cm, while the LAGP–PEO film maintains its integrity even when the ball is dropped from 40 cm (**Figure 3**a). This visual representation means the designed nacre-like composite electrolyte (NCE) is much tougher than the pure ceramic film.

Besides qualitative ball-dropping tests, the stiffness and strength of the LAGP–PEO NCPE film are quantitatively determined by three-point flexural tests. The LAGP–PEO film has a high ultimate flexural strength of 30.2 MPa, slightly lower than that of pure LAGP film (34.3 MPa, Figure 3b), but are ≈30 times higher than the PEO polymer (≈1 MPa) (Figure S5, Supporting Information). Furthermore, the failure strain for LAGP–PEO is roughly 1.1%, about one order of magnitude higher than that of pure LAGP film (0.13%). This is consistent with the layer-by-layer fracture behavior but not straight crack shown in previous work,[46,47] which also shows the nonlinear and step-like behavior. Compared to pure LAGP with a flexural modulus of 25.6 GPa, the LAGP–PEO, LAGP–PEA, and LAGP–epoxy NCPEs film are more flexible with lower flexural modulus of 7.8, 7.2, and 4.5 GPa, respectively (Figure 3c), but these values are significantly higher than that of pure polymer electrolyte and composite electrolytes (96 MPa[25] and 850 MPa[32]). Such enhanced mechanical strength and fracture strain originate from the synergic interaction of hard ceramic tablets and tough polymer interfacial layers arranged in the

Figure 2. Characterization of NCPEs. a) An optical image of as-fabricated LAGP–PEO NCPEs with a size of 5 cm × 5 cm. b) The volumetric percentage of LAGP ceramic in various NCPEs of LAGP–PEO, LAGP–PEA, and LAGP–epoxy. c,d) Cross-sectional SEM images of layered LAGP tablets before PEO infiltration and hot pressing (c) and an LAGP–PEO NCPE film showing the staggered microstructure after hot pressing (d).

Figure 3. Mechanical properties of NCPEs and toughening mechanisms. a) Impact test of as-fabricated LAGP–PEO NCPE and pure ceramic films, showing higher impact resistance in an LAGP–PEO NCPE film. The ball dropped from 20 cm for pure LAGP ceramic and from 40 cm height for NCPE, respectively. b) Flexural stress–strain curves of NCPEs and pure ceramic films through three-point bending tests. c) Young's modulus of NCPEs and pure ceramic. d,e) Vickers indentation of pure ceramic film and LAGP–PEO NCPE film using loads of 60 N (d) and 120 N (e). f,g) Nonlinear finite element simulations of: f) tortuous crack propagation through interfacial polymer failure in an NCPE film and g) a straight crack in a pure ceramic film under the same force load as in (f). h) Fractured surface of LAGP–PEO NCPE showing extensive interfacial failure. i) Optical images of ignition tests on pure PEO and LAGP–PEO NCPE films.

"brick-and-mortar" microstructure. In the future, with optimized annealing process to further enhance the mechanical strength of LAGP ceramic itself (e.g., to ≈100 MPa in common ceramics), the mechanical properties of NCPEs are expected to be further enhanced.

Additionally, other NCPE systems of LAGP–PEA and LAGP–epoxy NCEs exhibit similar enhancements in both mechanical strength and failure strain. When compared to their corresponding polymers, the ultimate flexural strengths increase from 0.06 to 20.4 MPa for LAGP–PEA, and from 1.5 to 25.6 MPa for LAGP–epoxy (Figure S5 in the Supporting Information for mechanical properties of pure polymer electrolytes). In the future, the mechanical properties can be further optimized by controlling the thickness of ceramic films and adjusting the pressure in the hot press.

Vickers indentation tests were further conducted to evaluate sample hardness and toughness. LAGP–PEO NCPE is selected as an example. Given that $HV = 0.1891F\,d^{-2}$, where HV is the hardness number, F is the applied load, and d is the diagonal left by the indenter, we find that the hardness for pure ceramic film (≈50 MPa) is higher than that for LAGP–PEO NCPE film (≈31 MPa) under the same load of $F = 60$ N (Figure 3d). This

agrees with results from three-bending tests in Figure 3b. However, under a load of $F = 120$ N, a long and straight crack of $L = 5$ mm is observed in pure LAGP film, while negligible crack initiation (<0.1 mm) but only a larger plastic indent is left in the NCPE film (Figure 3e). According to the well-known Evans–Charles formula for evaluating fracture toughness, $K_{IC} \propto 0.16\left(\dfrac{HV}{E}\right)^{-0.5} F\,L^{-1.5}$ (E is the modulus), the LAGP–PEO NCPE can accommodate more strain energy than pure ceramic.[48]

To determine mechanisms responsible for the improvement in toughness for nacre-like composite electrolytes, numerical simulation was carried out on crack propagation inside NCPEs with regular "brick-and-mortar" arrangement subjected to three-point bending. Figure 3f,g shows the stress distribution and crack propagation when a ceramic/polymer nacre-like film and a pure ceramic film with the same dimension undergo a fixed deflection of 1 mm, respectively. This displacement load corresponds to a flexural strain of 1.8% and can thus cause catastrophic failure in the pure ceramic film as a result of the straight crack since 1.8% is well beyond failure strain in ceramics (≈0.13%). For the nacre-like composite structure, however, the maximum stress in ceramic layers is only

**ADVANCED
SCIENCE NEWS**

www.advancedsciencenews.com

**ADVANCED
MATERIALS**

www.advmat.de
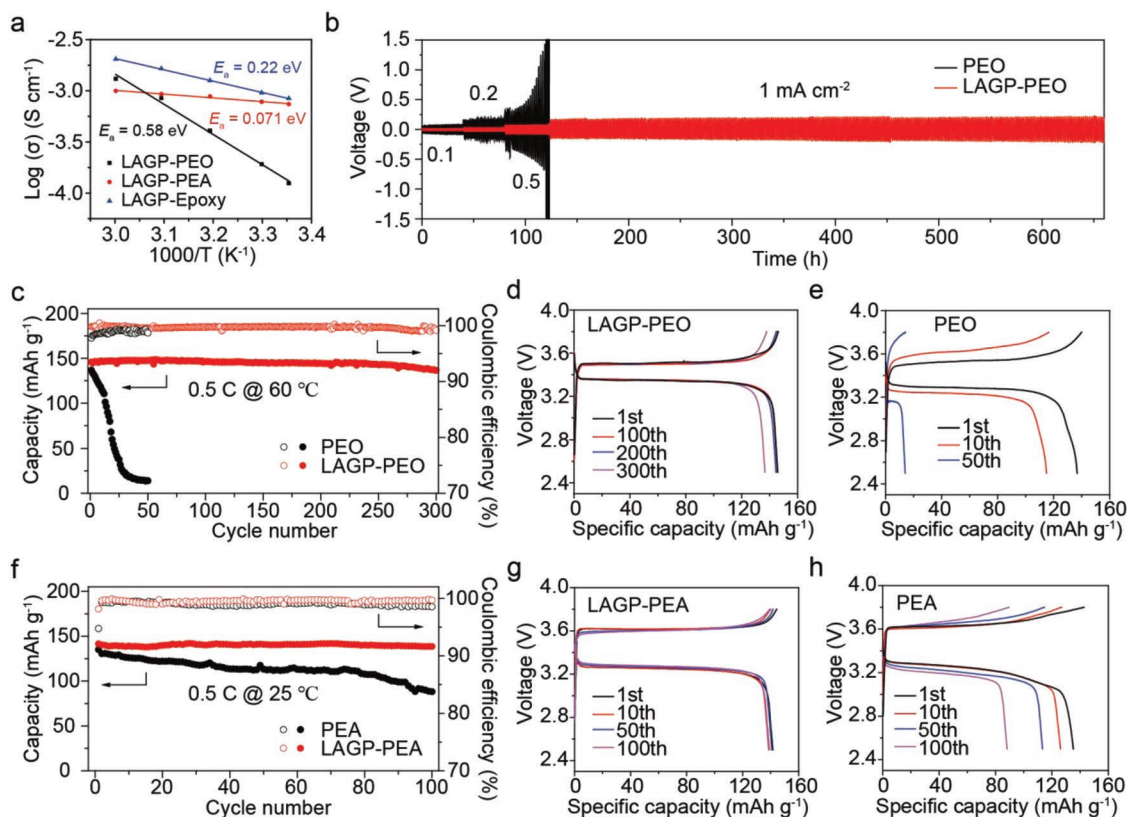
Figure 4. Electrochemical performances of NCPEs and NCPE-based full cells. a) The ionic conductivity versus temperature plot of NCPEs. b) Long-term cycling of Li/Li symmetric cells with pure PEO and LAGP–PEO NCPE at 60 °C with 1 mA cm^{-2} and 1 mAh cm^{-2}. c–e) Cycling performance of LFP/LAGP–PEO NCPE/Li and LFP/PEO/Li cells at 60 °C. f–h) Cycling performance of LFP/LAGP–PEA NCPE/Li and LFP/PEA/Li cells at 25 °C. In (c)–(h), the cells were charged and discharged at 0.5 C. The thickness of both LAGP–PEO, LAGP–PEA NCPEs and pure PEO, PEA electrolytes are 150 μm.

10 MPa, much less than the failure strength of ceramic. The stress release mechanism is the failure of interfacial polymer and the crack deflection at polymer interfaces with a torturous path, which does not propagate in the ceramic layer. The failed interfaces are subsequently dominated by interfacial sliding and plastic deformation, which toughens the composite and resists its catastrophic failure.[36,38] The SEM image of NCPEs' fractured surface (Figure 3h) illustrates extensive interfacial delamination between LAGP ceramic tablets and densely adhered polymer bridging, which confirms the efficient energy dissipation at interfaces. Both simulation and experimental evidence clearly show that NCPEs have advantages regarding flexibility and fracture toughness.

Furthermore, the LAGP–PEO NCPE film has high thermal stability and it does not ignite over the fire, as shown in Figure 3i and Video S1 in the Supporting Information. In contrast, pure PEO electrolyte can be ignited when exposed to a flame. This significant contrast further demonstrates the enhanced safety of NCPEs for battery applications. Through comparison of mechanical properties, the LAGP–polymer NCPEs outperforms to other state-of-the-art SSEs regarding ultimate flexural strength and fracture strain,[22,49–55] underpinning promising applications of the NCPE for safe, impact-resistant, and load-bearing batteries.

In addition to excellent mechanical properties, NCPEs also exhibit high ionic conductivity (**Figure 4**a). With the nacre-

like microstructure, the conductivity of LAGP–PEO NCPE reaches 1.25 × 10^{-4} S cm^{-1} at 25 °C and 1.3 × 10^{-3} S cm^{-1} at 60 °C in electrochemical impedance spectroscopy (EIS) tests (Figure S6, Supporting Information). This is much higher than the polymer phase itself (1.0 × 10^{-5} S cm^{-1} at 25 °C) and is close to that of pure LAGP pellet (2.0 × 10^{-4} S cm^{-1} at 25 °C), shown in Figure S7 in the Supporting Information. The value is also consistent with a simple parallel model of ceramic and polymer electrolytes based on their volume portion (Figure 2b), indicating low interfacial impedance. The conductivity of LAGP–PEO NCPE is also stable over 400 h (Figure S8, Supporting Information). The LAGP–PEA and LAGP–epoxy also exhibit ionic conductivities over 7.4 × 10^{-4} and 8.4 × 10^{-4} S cm^{-1} at room temperature (Figure 4a), respectively, which are close to the ionic conductivity of conventional liquid electrolytes with separator presented. The conductivities of pure PEA and epoxy electrolytes are also presented in Figure S7 in the Supporting Information. The high conductivities of NCPEs are attributed to the high volume portion of the conductive ceramic electrolyte and the small thickness of the interfacial polymer layer. The activation energies of these electrolytes have been calculated and listed in Table S2 in the Supporting Information. The as-fabricated LAGP–PEO NCPE possesses an activation energy (E_a) of 0.58 eV, which is much lower than 1.42 eV of pure PEO (25–40 °C), meaning that the

ADVANCED
SCIENCE NEWS
www.advancedsciencenews.com

ADVANCED
MATERIALS
www.advmat.de

lithium ion transport is dominated by the LAGP phase. For LAGP–PEA NCPE, its E_a (0.071 eV) is slightly higher than that of pure PEA electrolyte (0.069 eV) but much lower than that of LAGP tablet (0.40 eV). Similar condition is also found in LAGP–epoxy NCPE and epoxy electrolyte, displaying E_a of 0.22 and 0.20 eV, respectively. This is ascribed to that liquid electrolytes added inside the PEA and epoxy electrolytes facilitate the transport of lithium ions. In these electrolytes, lithium bis(trifluoromethanesulfonyl) imide (LiTFSI) is used in PEO and PEA systems and $LiClO_4$ is used in epoxy system, which are simply to show diversity of the proposed strategy.

To evaluate the electrochemical stability of NCPE, cyclic voltammetry (CV) was first executed in a stainless steel/LAGP–PEO/Li cell, which shows anodic stability up to 4.5 V versus Li/Li$^+$. Moreover, ≈150 µm thick LAGP–PEO NCPE was employed in symmetric Li/Li cells and tested at 60 °C. The Li/LAGP–PEO NCPE/Li cell was cycled at 0.1, 0.2, 0.5, and 1.0 mA cm^{-2} with 1 h charging and 1 h discharging, respectively. 7 µm separator is placed between Li and LAGP to avoid the reduction of LAGP by Li. The results clearly show that the overpotential of LAGP–PEO NCPE is steady, and only increases from 170 mV at the beginning to 204 mV after 500 h at 1.0 mA cm^{-2} and 1.0 mAh cm^{-2} (Figure 4b). This indicates that the lithium plating and stripping process is uniform, which is confirmed by the dense morphology of cycled lithium (Figure S9, Supporting Information). In contrast, the overpotential in the cell with pure PEO electrolyte increases dramatically and reaches the voltage limit of 1.5 V after 120 h at 0.5 mA cm^{-2}. The improved cycling stability of LAGP–PEA and LAGP–epoxy NCPEs compared to pure PEA and epoxy electrolytes are also demonstrated in Li/Li symmetric cells at room temperature (Figure S10, Supporting Information).

Although CV on stainless steel shows stability up to 4.5 V (Figure S11, Supporting Information), it should be noted that the stability window is largely determined by the substrate. On 4 V cathode (e.g., $LiCo_xNi_yMn_zO_2$) surface, PEO is easy to oxidize beyond 4 V versus Li/Li$^+$.[56] Hence, LFP is used as the cathode in full cell studies. The electrochemical performance of LAGP–PEO NCPE is further evaluated in an LFP/Li full cell at 60 °C and 0.5 C. The cell delivers an initial specific capacity of 145.8 mAh g^{-1}, which slightly increases to 148.5 mAh g^{-1} after 50 cycles, followed by a decay to 136.6 mAh g^{-1} after 300 cycles, corresponding to a capacity retention of 92%/300 cycles or 0.028% decay per cycle (Figure 4c). The average Coulombic efficiency (CE) is 99.7%. In contrast, the pure-PEO-based cell with the same electrolyte thickness experiences a significant capacity loss from 136.8 to 14 mAh g^{-1} after only 50 cycles, which possibly arises from the low conductivity of pure PEO electrolyte. Moreover, the LFP/LAGP–PEO NCPE/Li cell shows a stable overpotential of 0.16 V, while the overpotential of LFP/pure PEO/Li cell increases from 0.24 to 0.57 V after 50 cycles (Figure 4d,e).

The rate performance of cells with LAGP–PEO NCPE is also much better than that of pure PEO, featuring specific discharge capacity of 143.6, 136, and 100 mAh g^{-1} at 0.5, 1, and 2 C for LAGP–PEO NCPE, respectively (Figure S12, Supporting Information). Conversely, pure PEO features specific capacities of only 133.4, 92.8, and 2.5 mAh g^{-1} at 0.5, 1, and 2 C, respectively. The improved electrochemical performance of NCPE-based cells arises from NCPE's higher conductivity compared to pure PEO electrolyte.
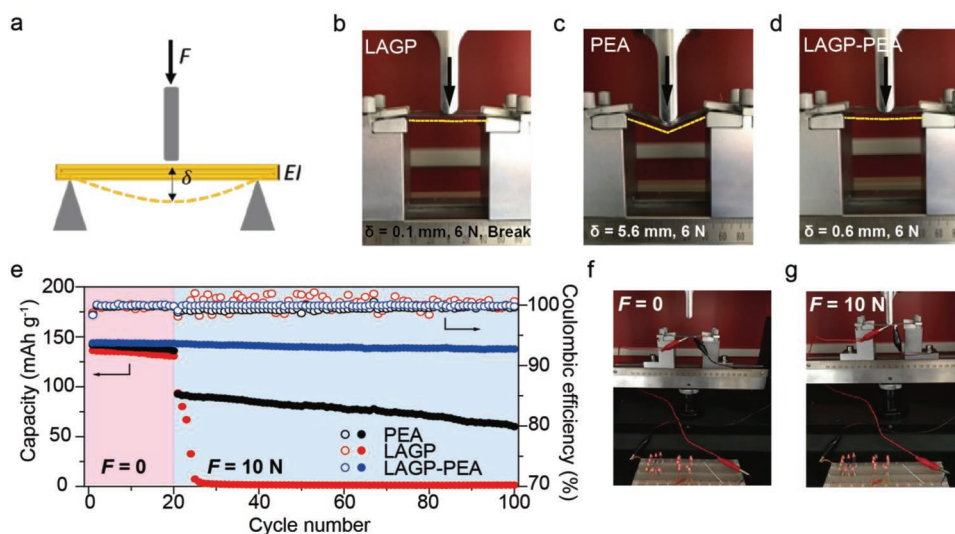
To further demonstrate operation at room temperature, we replaced PEO with PEA gel electrolyte, which provides higher conductivity of 7.4×10^{-4} S cm^{-1} at room temperature (Figure 4a). As shown in Figure 4f–h, high capacity retention of 97.9% and an average CE over 99.5% are obtained in LFP/LAGP–PEA/Li cell, while only 65.2% retention is observed after 100 cycles for electrolyte without LAGP. Such electrochemical reversibility at room temperature is critical for practical applications in solid-state batteries.

Another polymer electrolyte, epoxy, is further used to expand the family of polymer that could be used in nacre-like composite electrolytes. The LFP/Li cell with LAGP–epoxy NCPE delivers an initial specific capacity of 142.2 mAh g^{-1} at 0.3 C, followed by a slight decay to 132.3 mAh g^{-1} after 100 cycles, corresponding to capacity retention of 93.0% (Figure S14a,b, Supporting Information). Conversely, the cell with pure epoxy electrolyte exhibits a significant capacity drop from 143.8 to 72.7 mAh g^{-1} in 100 cycles with poor retention of 50.6% (Figure S14a,c, Supporting Information). Along with tests on nacre-like electrolytes, it should be noted that if polymer electrolyte is removed from the nacre structure, the electrolyte resistance will increase dramatically and corresponding LFP/Li cells can be barely cycled at 0.2 C, and leave no capacity at 0.5 C (Figure S15, Supporting Information).

To demonstrate enhanced stability of NCPEs under mechanical load, electrochemical cycling of NCPE-based cells under mechanical deformation is further carried out. First, pouch cells with the same electrolyte size of 5.3 cm × 2.3 cm × 0.5 mm but different electrolyte compositions (pure LAGP, pure PEA, and LAGP–PEA NCPE) are subjected to three-point bending tests (**Figure 5**a–d). When a force of 6 N is applied, the LFP/Li full cell with pure LAGP ceramic electrolyte breaks immediately with a small displacement of 0.1 mm (Figure 5b), as a result of the brittleness of ceramic. Moreover, the cell with pure PEA gel electrolyte shows a large deformation of 5.6 mm due to the softness of gel electrolytes (Figure 5c). In contrast, the cell with LAGP–PEA NCPE only exhibits a small deformation of 0.6 mm, 10% of that with gel electrolyte (Figure 5d). This indicates that the NCPE is much stiffer than the PEA electrolyte. Moreover, the NCPE does not break under such load, suggesting that it can absorb more energy than pure ceramic during deformation.

The enhanced mechanical properties of NCPEs are further validated by battery operation under mechanical deformation. Cells with electrolyte dimension of 53 × 53 × 0.5 mm^3 are subjected to the same point load of 10 N, corresponding to a high-stress level of 15 MPa in the NCPE electrolyte based on the flexural displacement. All electrode sizes are 5 cm × 5 cm with a capacity of 14 mAh, and the lithium thickness is 40 µm. Thin layers of PEA electrolyte are coated on the LFP cathode and Li anode for reducing interfacial resistance in all cells.

These cells with NCPE, LAGP, and PEA electrolytes are all cycled at 0.2 C for 20 cycles first, which show similar capacity and cycling performance (Figure 5e). However, once 10 N is applied, the capacity of the LAGP cell quickly drops to nearly zero after 3 cycles (Figure 5e; Figure S16a, Supporting Information), and the capacity of the PEA cell shows a sudden drop to 93.7 mAh g^{-1}, followed by a quick decay to 60.2 mAh g^{-1} after

**ADVANCED
SCIENCE NEWS**
www.advancedsciencenews.com

**ADVANCED
MATERIALS**
www.advmat.de

Figure 5. Mechanical stability of NCPE-based full cells. a) Schematic of indenting a suspended pouch cell under point force. b–d) Pouch cells with: b) pure LAGP under 0.1 mm displacement, c) pure PEA film under 6 N load, and d) LAGP–PEA NCPE under 0.6 mm displacement and 6 N load. e) The cycling performance of LFP/PEA/Li, LFP/LAGP/Li, and LFP/LAGP–PEA NCPE/Li cells at 0.2 C under point load of 10 N. f,g) A structural LFP/LAGP–PEA NCPE/Li pouch cell lighting a series of LEDs under no load (f) and 10 N load (g). 40 μm thin lithium was used in all these pouch cells.

100 cycles (Figure 5e; Figure S16b, Supporting Information). These results indicate that neither soft PEO nor brittle LAGP electrolyte can withstand external force. On the other side, the NCPE cell shows no apparent capacity loss after the load is applied, and the capacity retention is as high as 95.6% after 100 cycles. Stable CE of 99.9% and smooth voltage profiles are also achieved (Figure 5e; Figure S16c, Supporting Information). As a further demonstration, the NCPE cell can still power multiple LEDs after a point load of 10 N is applied (Figure 5f,g). Such significantly enhanced mechanical properties of NCPE ensure better stability in solid-state batteries against external impact. Results above also suggest that the nacre-like design is attractive for structural energy storage, where batteries are used to replace structural components in vehicles and aircraft for weight reduction but need to withstand high mechanical loads.[57,58]

In summary, we have fabricated nacre-like ceramic/polymer composite electrolytes with the "brick-and-mortar" microstructure, demonstrating both high ultimate flexural strength and high toughness (Table S3, Supporting Information), and resolving the dilemma between high strength/low toughness in pure ceramic electrolytes and low strength/high toughness in pure polymer electrolytes. The mechanically robust NCPEs allow high capacity retention of 95.6% over 100 cycles in an LFP/Li pouch cell, even when it is subjected to an external point load. In contrast, cells based on pure ceramic and pure polymer electrolytes show sudden capacity drop and quick fading when the same magnitude of the mechanical load is applied. Therefore, the proposed nacre-like configuration presents a promising load-bearing ceramic/polymer composite electrolyte for solid-state batteries and even structural energy storage with high energy density, excellent mechanical properties, and high thermal stability. Among the three nacre-like electrolytes above, LAGP–PEO has the highest mechanical strength and modulus while LAGP–PEA has better cycling performance than the

epoxy system. As LAGP–PEO does not work well at RT, we consider LAGP–PEA has a balanced and most attractive performance among these three systems.

Experimental Section

Synthesis of LAGP Flake: LAGP ceramic powder was purchased from MTI Corporation and used as received. Tape casting was used to fabricate the brick of the multilayer LAGP. The LAGP powder with fish oil as a dispersant was added to toluene and isopropanol, followed by 1 h of sonication and 12 h of sintering. Then, binder and plasticizers were added and stirred for another 12 h. The detailed composition is listed in Table S4 in the Supporting Information. The slurry was degassed in a vacuum oven for 5 min before use. Then, the slurry was tape cast by an applicator, through which the slurry would be pulled out as a thin film. The resulting film was cut into pieces, laminated together, and dried at 120 °C for 1 h. The samples were presintered at 500 °C for 1 h to remove the organic component and then sintered at 850 °C for 6 h with a heating rate of 2.5 °C min^{-1}.

Synthesis of Nacre-Like Ceramic/Polymer Electrolytes: Three different kinds of polymers were used to prepare the nacre-like ceramic/polymer electrolytes, including PEO (M_w = 600 000), PEA, and epoxy. LAGP–PEO electrolytes were synthesized by the infiltration process. Specifically, lithium bis(trifluoromethanesulfonyl) imide (LiTFSI, Sigma-Aldrich), polyethylene glycol dimethyl ether (PEGDME, Sigma-Aldrich), and PEO (PEO:PEGDME = 2:1, by weight; EO:Li = 16:1, by molar) were dissolved into acetonitrile and infiltrated into the gaps between LAGP bricks under vacuum, and then dried to evaporate the solvent. LAGP–PEA ceramic/polymer electrolytes were prepared by ultraviolet curing. The precursor of monomer (ethoxylated trimethylolpropane triacrylate, M_w = 428, Sigma-Aldrich), photoinitiator (2-hydroxy-2-methyl-1-phenyl-1-propanon, Sigma-Aldrich), liquid electrolyte (1 M LiTFSI in 1,3-dioxolane (DOL) and 1,2-dimethoxyethane (DME) (DOL:DME = 1:1, by volume)), and PEO (2.5 wt%, dissolved in anhydrous dimethyl sulfoxide) were mixed with the volume ratio of 1/1.5/1.5, wherein the photoinitiator was fixed at 1.0 wt% of monomer. Then, the mixture was infiltrated into LAGP flakes and cured for about 5 min. For the synthesis of LAGP–epoxy electrolytes, liquid electrolyte (1 M LiClO₄ in propylene carbonate (PC)) was mixed

with epoxy resin and epoxy hardener with a weight ratio of 1/0.5/0.5, and subsequently infiltrated into multilayer-LAGP and baked at 70 °C for 12 h. Then, the LAGP–epoxy electrolyte was soaked in 1 M LiClO$_4$/PC for 12 h. After assembling, the nacre-like ceramic/polymer electrolytes were hot-pressed at 80 °C to help further infiltration into gaps between ceramic platelets.

Material Characterizations: Crystal structures were collected by a PANalytical XPert3 Powder XRD with Cu Kα radiation run at 45 mA and 40 V. Morphology of samples was characterized with SIGMA VP Zeiss scanning electron microscopy at 5.0 kV. The ratios of ceramic LAGP to polymer were determined by a TA Instruments Q 500 TGA with a temperature-rising speed of 10 °C min^{-1} over the entire temperature range from 25 to 600 °C in oxygen.

Mechanical Tests: For ball impact tests, a home-made setup including a plastic tube and a stainless steel sphere of 8.4 g weight falling freely from 20 or 40 cm height was used. All samples were 1 mm thick for NCPEs and ceramic films. Flexural tests of three-point bending were conducted on SANS-UTM 6000 using 200 N load cells. The specimens of NCPEs, polymer electrolytes, and ceramic electrolytes were cut with a thickness of 500 μm and a size of 1.5 cm. A loading rate of 0.5 mm min^{-1} and a support span of 1.5 cm were used in all tests. The results were averaged from those in five similar specimens. The flexural stress is $\sigma_f = \frac{3FL}{2wh^2}$ and the flexural strain is $\varepsilon_f = \frac{6Dh}{L^2}$, where F, L, w, h, and D are the applied point force, span length, sample width, thickness, and flexural deflection, respectively. Vickers indentation was carried out on SANS-UTM 6000 using a Vickers indenter.

Finite Element Mechanical Simulation: 2D nonlinear finite element simulations were conducted using the software ABAQUS v6.14. In these simulations, the stress/strain distributions and crack propagation in a regular brick–mortar structure and a ceramic film are calculated by modeling three-point bending. The two bottoms support with a span of 4 mm were fixed and the loading was applied at the center of top indentation with a displacement load of 100 μm. A vertical and straight notch of 50 μm at the bottom middle point was set in both structures to initiate crack propagation. The "brick-and-mortar" structure contains a regular staggered arrangement of ceramic tablet (200 μm × 20 μm) bricks bonded by the thin layer of polymer (thickness of 1 μm). The polymer layer was modeled as a cohesive zone with a bilinear traction separation and underwent friction after damage, and the modulus was set to E_p = 10 MPa with the Poison ratio of = 0.47, and the failure strain of 10%. The bricks were modeled as brittle materials with the isotropic bulk modulus E_p = 20 GPa, Poison ratio of 0.33, and failure strength of 55 MPa before brittle failure. After reaching the failure strength, the traction separation for ceramic elements was still assumed to be linear until the strain up to 0.25%. CPE4 elements were used in all models and the convergence study verified the mesh size of 0.5 μm for polymer elements and 2 μm for ceramic elements, from which both correction and computational efficiency can be obtained.

Battery Assembly: LFP cathode was prepared by mixing LFP powder (d'Hydro-Québec), SUPER C65 conductive carbon (Timcal), poly (vinylidene fluoride) (Kynar 761, Arkema), and LiTFSI with a mass ratio of 8:1:1:1 in N-methyl-2-pyrrolidone (99%, Sigma-Aldrich) to form a homogeneous slurry. Then, the slurry was coated on an aluminum foil and dried overnight at 110 °C. CR2032 coin-type and pouch-type cells were assembled with a mass loading of ≈4 mg cm^{-2}. Lithium metal with a thickness of 250 and 40 μm were utilized in coin cell and pouch cell, respectively. To prevent the reduction of LAGP by lithium metal, one piece of polyethylene separator (Clegard, 7 μm) was applied between lithium anode and the solid-state electrolytes. All of the cells, including stainless steel/Li cells, Li/Li symmetric cells, and LFP/Li cells, were assembled in an argon-filled glove box with moisture and oxygen levels below 0.1 and 1 ppm, respectively.

Electrochemical Measurements: EIS was conducted on a VMP3 multichannel potentiostat from Bio-Logic using 20 mV amplitude with a frequency range from 1 MHz to 0.1 Hz. CV of stainless steel/Li cell was also executed on Bio-Logic from −0.5 to 4.5 V with a scanning speed of 0.1 mV s^{-1}. Galvanostatic cycling was performed by the Wuhan Landt

tester. The voltage cut-off of LFP/Li cell was fixed at 2.5–3.8 V. The battery performance tests utilizing LAGP–PEO electrolyte were conducted at 60 °C, while cells using LAGP–PEA and LAGP–epoxy electrolytes were tested at room temperature.

Supporting Information

Supporting Information is available from the Wiley Online Library or from the author.

Acknowledgements

Conflict of Interest

The authors declare no conflict of interest.

Keywords

[1] S. Xia, X. Wu, Z. Zhang, Y. Cui, W. Liu, *Chem* **2018**, *5*, 753.

[2] M. S. Whittingham, *Chem. Rev.* **2004**, *104*, 4271.

[3] J. B. Goodenough, K. S. Park, *J. Am. Chem. Soc.* **2013**, *135*, 1167.

[4] B. Liu, J.-G. Zhang, W. Xu, *Joule* **2018**, *2*, 833.

[5] Y. K. Sun, S. T. Myung, B. C. Park, J. Prakash, I. Belharouak, K. Amine, *Nat. Mater.* **2009**, *8*, 320.

[6] D. Lin, Y. Liu, Y. Cui, *Nat. Nanotechnol.* **2017**, *12*, 194.

[7] L. Fan, S. Wei, S. Li, Q. Li, Y. Lu, *Adv. Energy Mater.* **2018**, *8*, 1702657.

[8] M. Dirican, C. Yan, P. Zhu, X. Zhang, *Mater. Sci. Eng., R* **2019**, *136*, 27.

[9] J. Wan, J. Xie, D. G. Mackanic, W. Burke, Z. Bao, Y. Cui, *Mater. Today Nano* **2018**, *4*, 1.

[10] J. Fu, *Solid State Ionics* **1997**, *104*, 191.

[11] Q. Cheng, A. Li, N. Li, S. Li, A. Zangiabadi, W. Huang, A. C. Li, T. Jin, Q. Song, W. Xu, *Joule* **2019**, *3*, 1510.

[12] H. Aono, E. Sugimoto, Y. Sadaoka, N. Imanaka, G.-y. Adachi, *J. Electrochem. Soc.* **1990**, *137*, 1023.

[13] F. Han, Y. Zhu, X. He, Y. Mo, C. Wang, *Adv. Energy Mater.* **2016**, *6*, 1501590.

[14] S.-S. Chi, Y. Liu, N. Zhao, X. Guo, C.-W. Nan, L.-Z. Fan, *Energy Storage Mater.* **2019**, *17*, 309.

[15] N. Kamaya, K. Homma, Y. Yamakawa, M. Hirayama, R. Kanno, M. Yonemura, T. Kamiyama, Y. Kato, S. Hama, K. Kawamoto, *Nat. Mater.* **2011**, *10*, 682.

**ADVANCED
SCIENCE NEWS**

www.advancedsciencenews.com

**ADVANCED
MATERIALS**

www.advmat.de

[16] F. Mizuno, A. Hayashi, K. Tadanaga, M. Tatsumisago, *Adv. Mater.* **2005**, *17*, 918.

[17] Z. Deng, Z. Wang, I.-H. Chu, J. Luo, S. P. Ong, *J. Electrochem. Soc.* **2016**, *163*, A67.

[18] S. Yu, R. D. Schmidt, R. Garcia-Mendez, E. Herbert, N. J. Dudney, J. B. Wolfenstine, J. Sakamoto, D. J. Siegel, *Chem. Mater.* **2015**, *28*, 197.

[19] Z. Xue, D. He, X. Xie, *J. Mater. Chem. A* **2015**, *3*, 19218.

[20] K. J. Harry, D. Y. Parkinson, N. P. Balsara, *JoVE* **2015**, *102*, 53021.

[21] P. Barai, K. Higa, V. Srinivasan, *J. Electrochem. Soc.* **2017**, *164*, A180.

[22] L. Chen, Y. Li, S.-P. Li, L.-Z. Fan, C.-W. Nan, J. B. Goodenough, *Nano Energy* **2018**, *46*, 176.

[23] S. Choudhury, R. Mangal, A. Agrawal, L. A. Archer, *Nat. Commun.* **2015**, *6*, 10101.

[24] I. Villaluenga, K. H. Wujcik, W. Tong, D. Devaux, D. H. Wong, J. M. DeSimone, N. P. Balsara, *Proc. Natl. Acad. Sci. USA* **2016**, *113*, 52.

[25] P. Yao, B. Zhu, H. Zhai, X. Liao, Y. Zhu, W. Xu, Q. Cheng, C. Jayyosi, Z. Li, J. Zhu, *Nano Lett.* **2018**, *18*, 6113.

[26] S.-O. Tung, S. Ho, M. Yang, R. Zhang, N. A. Kotov, *Nat. Commun.* **2015**, *6*, 6152.

[27] D. Li, L. Chen, T. Wang, L.-Z. Fan, *ACS Appl. Mater. Interfaces* **2018**, *10*, 7069.

[28] S. Song, Y. Wu, W. Tang, F. Deng, J. Yao, Z. Liu, R. Hu, Alamusi, Z. Wen, L. Lu, N. Hu, *ACS Sustainable Chem. Eng.* **2019**, *7*, 7163.

[29] D. Lin, P. Y. Yuen, Y. Liu, W. Liu, N. Liu, R. H. Dauskardt, Y. Cui, *Adv. Mater.* **2018**, *30*, 1802661.

[30] H. Zhai, P. Xu, M. Ning, Q. Cheng, J. Mandal, Y. Yang, *Nano Lett.* **2017**, *17*, 3182.

[31] X. Wang, H. Zhai, B. Qie, Q. Cheng, A. Li, J. Borovilas, B. Xu, C. Shi, T. Jin, X. Liao, *Nano Energy* **2019**, *60*, 205.

[32] J. Wan, J. Xie, X. Kong, Z. Liu, K. Liu, F. Shi, A. Pei, H. Chen, W. Chen, J. Chen, X. Zhang, L. Zong, J. Wang, L.-Q. Chen, J. Qin, Y. Cui, *Nat. Nanotechnol.* **2019**, *14*, 705.

[33] C.-Z. Zhao, X.-Q. Zhang, X.-B. Cheng, R. Zhang, R. Xu, P.-Y. Chen, H.-J. Peng, J.-Q. Huang, Q. Zhang, *Proc. Natl. Acad. Sci. USA* **2017**, *114*, 11069.

[34] N. Shirshova, H. Qian, M. Houllé, J. H. G. Steinke, A. R. J. Kucernak, Q. P. V. Fontana, E. S. Greenhalgh, A. Bismarck, M. S. P. Shaffer, *Faraday Discuss.* **2014**, *172*, 81.

[35] H.-B. Yao, H.-Y. Fang, X.-H. Wang, S.-H. Yu, *Chem. Soc. Rev.* **2011**, *40*, 3764.

[36] H. L. Gao, S. M. Chen, L. B. Mao, Z. Q. Song, H. B. Yao, H. Colfen, X. S. Luo, F. Zhang, Z. Pan, Y. F. Meng, Y. Ni, S. H. Yu, *Nat. Commun.* **2017**, *8*, 287.

[37] L. B. Mao, H. L. Gao, H. B. Yao, L. Liu, H. Colfen, G. Liu, S. M. Chen, S. K. Li, Y. X. Yan, Y. Y. Liu, S. H. Yu, *Science* **2016**, *354*, 107.

[38] Y. Ni, Z. Song, H. Jiang, S.-H. Yu, L. He, *J. Mech. Phys. Solids* **2015**, *81*, 41.

[39] F. Barthelat, *J. Mech. Phys. Solids* **2014**, *73*, 22.

[40] L. Shao, J.-W. Jeon, J. L. Lutkenhaus, *Chem. Mater.* **2011**, *24*, 181.

[41] S. Ekstedt, M. Wysocki, L. Asp, *Plast., Rubber Compos.* **2010**, *39*, 148.

[42] A. Manthiram, X. Yu, S. Wang, *Nat. Rev. Mater.* **2017**, *2*, 16103.

[43] X.-X. Zeng, Y.-X. Yin, N.-W. Li, W.-C. Du, Y.-G. Guo, L.-J. Wan, *J. Am. Chem. Soc.* **2016**, *138*, 15825.

[44] C. S. Choi, J. Lau, J. Hur, L. Smith, C. Wang, B. Dunn, *Adv. Mater.* **2018**, *30*, 1703772.

[45] J. I. Hur, L. C. Smith, B. Dunn, *Joule* **2018**, *2*, 1187.

[46] S. Zekoll, C. Marriner-Edwards, A. O. Hekselman, J. Kasemchainan, C. Kuss, D. E. Armstrong, D. Cai, R. J. Wallace, F. H. Richter, J. H. Thijssen, *Energy Environ. Sci.* **2018**, *11*, 185.

[47] M. Morits, T. Verho, J. Sorvari, V. Liljeström, M. A. Kostiainen, A. H. Gröschel, O. Ikkala, *Adv. Funct. Mater.* **2017**, *27*, 1605378.

[48] Y. Feng, T. Zhang, R. Yang, *J. Am. Ceram. Soc.* **2011**, *94*, 332.

[49] D. Lin, P. Y. Yuen, Y. Liu, W. Liu, N. Liu, R. H. Dauskardt, Y. Cui, *Adv. Mater.* **2018**, *30*, e1802661.

[50] S.-H. Kim, K.-H. Choi, S.-J. Cho, J. Yoo, S.-S. Lee, S.-Y. Lee, *Energy Environ. Sci.* **2018**, *11*, 321.

[51] S. Zekoll, C. Marriner-Edwards, A. K. O. Hekselman, J. Kasemchainan, C. Kuss, D. E. J. Armstrong, D. Cai, R. J. Wallace, F. H. Richter, J. H. J. Thijssen, P. G. Bruce, *Energy Environ. Sci.* **2018**, *11*, 185.

[52] P. Yao, B. Zhu, H. Zhai, X. Liao, Y. Zhu, W. Xu, Q. Cheng, C. Jayyosi, Z. Li, J. Zhu, K. M. Myers, X. Chen, Y. Yang, *Nano Lett.* **2018**, *18*, 6113.

[53] D. Lin, W. Liu, Y. Liu, H. R. Lee, P.-C. Hsu, K. Liu, Y. Cui, *Nano Lett.* **2016**, *16*, 459.

[54] W. Liu, S. W. Lee, D. Lin, F. Shi, S. Wang, A. D. Sendek, Y. Cui, *Nat. Energy* **2017**, *2*, 17035.

[55] K. K. Fu, Y. Gong, J. Dai, A. Gong, X. Han, Y. Yao, C. Wang, Y. Wang, Y. Chen, C. Yan, Y. Li, E. D. Wachsman, L. Hu, *Proc. Natl. Acad. Sci. USA* **2016**, *113*, 7094.

[56] H. Zhai, T. Gong, B. Xu, Q. Cheng, D. Paley, B. Qie, T. Jin, Z. Fu, L. Tan, Y.-H. Lin, *ACS Appl. Mater. Interfaces* **2019**, *11*, 28774.

[57] G. Qian, X. Liao, Y. Zhu, F. Pan, X. Chen, Y. Yang, *ACS Energy Lett.* **2019**, *4*, 690.

[58] P. Ladpli, R. Nardari, F. Kopsaftopoulos, Y. Wang, F.-K. Chang, presented at *8th European Workshop on Structural Health Monitoring (EWSHM 2016)*, Bilbao, Spain, July **2016**.